Teleseismic double-difference relocation of earthquakes along the Sumatra-Andaman subduction zone using a 3-D model

J. D. Pesicek,[1] C. H. Thurber,[1] H. Zhang,[2] H. R. DeShon,[3] E. R. Engdahl,[4] and S. Widiyantoro[5]

Received 3 February 2010; revised 7 May 2010; accepted 28 May 2010; published 8 October 2010.

[1] We have extended the double-difference seismic tomography method to teleseismic distances with 3-D ray tracing conducted through nested regional-global velocity models and applied the method to relocate seismicity from the Sumatra-Andaman region before and after the great earthquakes of 2004 and 2005. We tested the algorithm's accuracy using both independent local data and an alternate relocation method and found good agreement between the results. The use of depth phases, differential times, and a realistic 3-D velocity model improves the accuracy and precision of epicenters and focal depths, systematically shifting them perpendicular to the trench and shallower, respectively. The relocations refine the location of the megathrust and other faults, the patterns of aftershocks, and their relation to slip during the two great earthquakes. In addition, the relocations reveal several discrete features not readily discernible in the scatter of teleseismic catalogs, including an arcuate, narrow band of earthquakes presumed to define the updip rupture limit in the 2005 event and a lineation at depth tracing the subduction of the Investigator Fracture Zone. When viewed in conjunction with tomography results, the geometry and structural features of the subduction zone are revealed in unprecedented detail.

Citation: Pesicek, J. D., C. H. Thurber, H. Zhang, H. R. DeShon, E. R. Engdahl, and S. Widiyantoro (2010), Teleseismic double-difference relocation of earthquakes along the Sumatra-Andaman subduction zone using a 3-D model, *J. Geophys. Res.*, *115*, B10303, doi:10.1029/2010JB007443.

1. Introduction

[2] The Sumatra and Andaman Islands region is currently one of the most seismically active areas in the world. The subduction megathrust has generated three great earthquakes in recent years: 26 December 2004 Mw 9.1 Sumatra-Andaman Islands, 28 March 2005 Mw 8.7 Nias Island, and 12 September 2007 Mw 8.4 Southern Sumatra events. These earthquakes have spawned countless aftershocks within the shallow subduction zone, including thousands of $M > 5$ and additional large $M > 7$ earthquakes but also triggered seismicity along the outer rise, the Andaman back arc, within the upper plate, and at intermediate depths (Figure 1) [*Dewey et al.*, 2007; *Engdahl et al.*, 2007; *Sieh et al.*, 2008]. However, like many subduction environments, local seismic station coverage is quite limited along strike of this archipelago and along dip of the entire seismogenic zone. Although coverage from the few land-based seismic stations has been supplemented by several deployments of ocean bottom seismometers (OBS) following the 2004 great Sumatra-Andaman Islands earthquake [*Araki et al.*, 2006; *Lin et al.*, 2009; *Tilmann et al.*, 2010], these data sets are limited both spatially and temporally. The sum of these local data falls short of providing a regional earthquake location catalog that covers ~2000 km of plate boundary. As more geological and geophysical information becomes available for the margin, high-precision regional relocations will allow for discrimination between interplate and intraplate source regions and allow for comparison between seismicity and thermal, mechanical, compositional, and rupture models of the Sunda margin.

[3] Catalogs of arrivals at teleseismic stations provide the most consistent and reliable data sets for analysis of seismicity prior to and following the 2004 and 2005 great earthquakes. Global catalogs of such data are produced and routinely updated by International Seismic Center (ISC) and National Earthquake Information Center (NEIC). Analyses of these data yield primary constraints on slab and fault geometries, regional spatiotemporal patterns of seismicity, and information on the extent of the seismogenic zone within the

[1]Department of Geoscience, University of Wisconsin-Madison, Madison, Wisconsin, USA.
[2]Department of Earth, Atmospheric and Planetary Sciences, Massachusetts Institute of Technology, Cambridge, Massachusetts, USA.
[3]Center for Earthquake Research and Information, University of Memphis, Memphis, Tennessee, USA.
[4]Department of Physics, University of Colorado at Boulder, Boulder, Colorado, USA.
[5]Faculty of Mining and Petroleum Engineering, Bandung Institute of Technology, Bandung, Indonesia.

0148-0227/10/2010JB007443

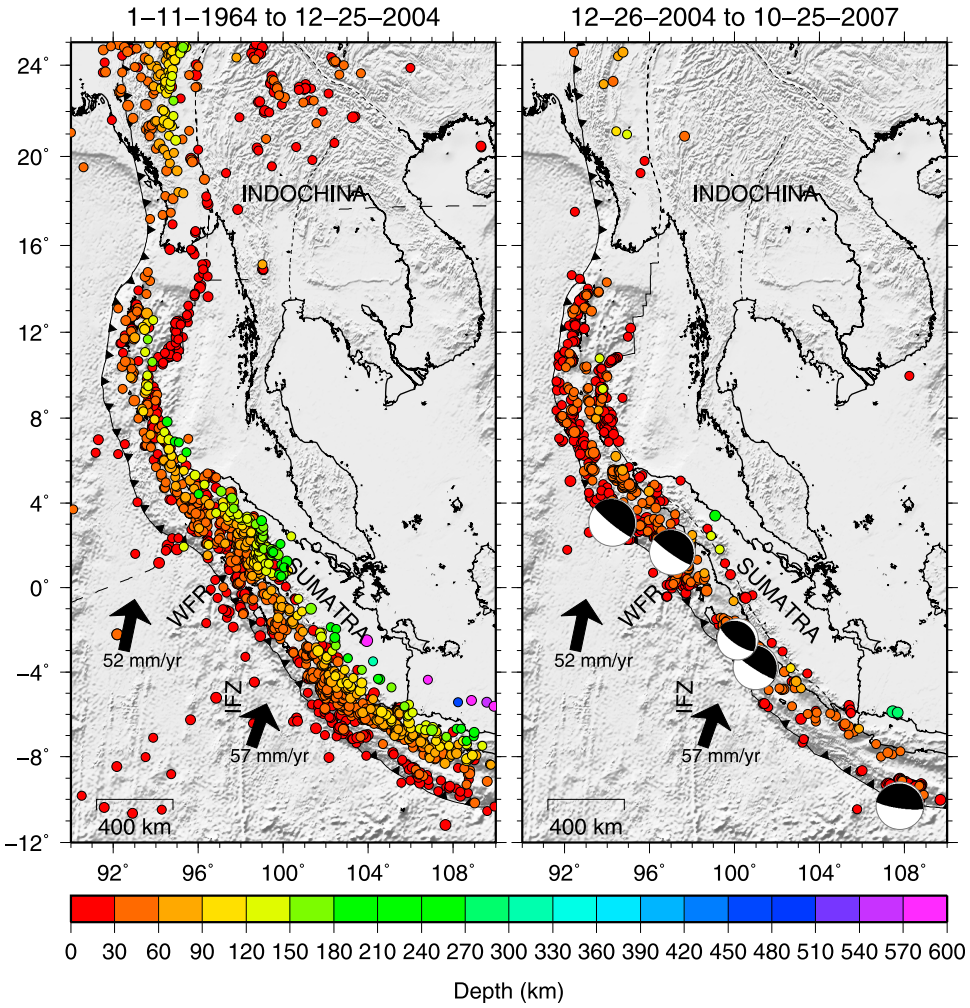

Figure 1. Distribution of EHB earthquakes with $m_b > 5$ (1964–2007) relocated in this study. (left) Events prior to the 2004 great earthquake and (right) events that occurred after it. Also shown are the Investigator Fracture Zone (IFZ), Wharton Fossil Rift (WFR), global CMTs for events with Mw > 7.75, and plate motion vectors [*Sieh and Natawidjaja*, 2000].

Sumatra-Andaman subduction system [*Dewey et al.*, 2007; *Engdahl et al.*, 2007]. However, typical scatter in single-event teleseismic locations limits delineation of the fine-scale structural features of the seismogenic zone and hinders efforts to gain further insight into the tectonic setting in which these two great earthquakes occurred.

[4] Significant improvements to the resolution of teleseismic catalogs have been achieved by reprocessing of the ISC and NEIC global data using the Engdahl, van der Hilst, and Buland (EHB) method of single-event relocation [*Engdahl et al.*, 1998]. The EHB catalog is commonly recognized as the most accurate catalog of event locations available for global seismic studies. The method employs a variety of strategies to increase the accuracy of the teleseismic data, including iterative relocation with dynamic phase identification, weighting phase data as a function of model uncertainty variance with epicentral distance, and ellipticity and station patch corrections. In the Sumatra-Andaman region, teleseismic data prior to and following the 2004 and 2005 great earthquake sequences have been refined by the EHB method, reducing estimated epicenter and focal depth uncertainties to roughly 15 and 10 km, respectively [*Engdahl et al.*, 2007]. Despite these improvements, the precision of the EHB locations remains inherently limited by the quality of the ISC and NEIC data. Errors in phase identification and arrival time picks and absolute velocity model errors contribute directly to location errors.

[5] The effects of data errors that limit single-event relocation techniques can be suppressed by the use of multiple event relocation techniques that minimize common path errors, producing precise relative arrival times. In this study, we attempted to improve upon the comprehensive EHB catalog of seismicity in the Sumatra-Andaman region by applying a multiple-event double-difference (DD) relocation technique with a 3-D velocity model to teleseismically recorded events that occurred along the Burma, Andaman, and Sumatra subduction zones from 1964 through 2007. We selected ~8000 well-constrained EHB events for relocation. Specifically, we required a teleseismic secondary azimuthal gap <180°, and we only used events that were well constrained in depth. This depth control was achieved by using later arriving phases in addition to first arriving *P* phases

that were dynamically reidentified as depth phases (*pP*, *pwP*, and *sP*) by the EHB location algorithm. First arriving *P* phases alone only provide sufficient depth constraint if the distance of the station to the event is within a focal depth (i.e., an upgoing *P* ray). The inclusion of depth phases is advantageous because their travel-time derivatives for depth are opposite in sign to that of direct *P*, and thus, they can help reduce the tradeoff between origin time and depth, thereby better constraining focal depth. The improved precision of the DD relocations allows refinement of slab and megathrust geometry, improved characterization of the spatiotemporal seismicity patterns associated with the rupture limits of the 2004 and 2005 great earthquakes, and discussion of seismically identified incoming plate structural features, such as the Investigator Fracture Zone (IFZ), at intermediate depths.

2. Teleseismic Double-Difference Earthquake Relocation

[6] Double-difference (DD) techniques have been applied to a variety of earthquake relocation problems in recent years. The original DD method [*Waldhauser and Ellsworth*, 2000] has proven effective at determining precise relative local and regional earthquake locations within many seismic networks [e.g., *Prejean et al.*, 2002; *Schaff et al.*, 2002; *Waldhauser and Ellsworth*, 2002; *Fukuyama et al.*, 2003]. When adapted to determine the 3-D velocity structure and absolute event locations in addition to relative locations [*Zhang and Thurber*, 2003], the DD method has provided high-resolution tomographic images and high-precision event locations at a variety of scales and in a variety of tectonic settings [*Zhang and Thurber*, 2006]. More recently, the DD relocation method (using a 1-D model) has been successfully applied at teleseismic distances as well [*Waldhauser and Schaff*, 2007].

[7] In order to relocate seismicity from the Sumatra-Andaman region in an optimal manner, we have extended the DD tomography algorithm *tomoDD* of *Zhang and Thurber* [2003] to teleseismic distances (*teletomoDD*). The key modification of the algorithm required for teleseismic relocation was the addition of a spherical Earth ray tracer for a 3-D model. To determine raypaths and calculate travel times in a spherical earth, we have utilized the pseudobending (PB) method of *Um and Thurber* [1987], extended to a spherical Earth with discontinuities by *Koketsu and Sekine* [1998]. To account for heterogeneous velocity structure both inside and outside the region of interest, travel times are calculated through 3-D nested regional-global models represented as perturbations relative to the radially symmetric global model *ak135* [*Kennett et al.*, 1995]. In the Sumatra region, rays are traced through the 0.5° *P* wave velocity model of *Pesicek et al.* [2010], whereas outside the regional model, they are traced through the *MITP08* global *P* wave perturbation model [*Li et al.*, 2008]. Unmodeled velocity structure beyond that accounted for by the nested 3-D models is further mitigated by the use of station corrections. In addition to tracing rays for primary phases, we have modified the PB ray tracer to also trace rays for the depth phases *pP* and *pwP*. We traced depth phases initially to the EHB catalog bounce points, which were then iteratively perturbed until the angles between the upgoing and downgoing ray segments are equivalent [*Zhao and Lei*, 2004].

[8] Where broadband waveforms exist, we used a frequency-based automatic picking technique to identify additional first arrivals and depth phase onset times for inclusion in the data set [*DeShon et al.*, 2007]. In this approach, we calculated the power spectral density (PSD) function at 1 Hz for velocity and displacement time series. The PSD time series reflects the magnitude of the discrete Fourier transform calculated using a second-order Goertzel algorithm at 1 Hz and is derived using a two-sample Hamming window with a 1 s overlap. The small window allows for increased time resolution at the cost of spectral leakage. We then took the gradient of the resultant velocity and displacement time series, applied minimum smoothing, and normalized the series to 1.0. In order to more easily identify changes in the gradient time series associated with arriving phases, points less than the mean are set to zero. This admittedly limits our ability to identify emergent arrivals. Abrupt changes in the gradient occurring on both time series were then associated with *P*, *pP*, or *sP*. Depth phase picks were not allowed to deviate by more than 2–3 s from the theoretical time based on the initial EHB location. This criterion assumes catalog quality of 10–15 km in depth and decreases the number of overall triggers to limit false positives in the *P* coda. The technique results in 57,388 *P*, 23,715 *pP*, and 7,404 *pwP* picks for use with the DD method.

[9] To improve pick precision and to calculate precise relative arrival times for inclusion in the DD relocation, we have also applied cross-correlation (CC) techniques to the waveform data (Figure 2) [*Du et al.*, 2004; *DeShon et al.*, 2007]. Correlation of *P* and *pP* phases was calculated in both the second-order and third-order spectral domains (i.e., standard cross correlation and bispectrum correlation) to maximize robustness of the correlation results and to reduce noise effects. Teleseismic waveforms were bandpass filtered between 0.5 and 5 Hz. Correlation was calculated using windows 1 s prior to and 2.5 s after the *P* onset and 4 s prior to and 4 s after the *pP* onset. A broad window was used to allow for poorly picked depth phase onsets in the original EHB catalog, which relies on analyst reports from the ISC and NEIC. The adjusted picks were used to form precise differential times for input into the DD relocation procedure.

[10] With the additional depth phase and CC data, we have included six different data types in the relocation procedure: primary and depth phase absolute data, primary and depth phase catalog differential times, and primary and depth phase CC differential times. To form the catalog differential times, we followed *Waldhauser and Schaff* [2007] and linked each event with its 20 nearest neighbors within 300 km that had at least 15 commonly observed phases at stations within 90°, requiring a minimum of 10 differential time links per pair. Owing to the importance of the depth phase data for constraining focal depth despite their relative paucity, we relaxed these conditions and required only two links per neighbor and two links per pair to form depth phase differential times. In total, we have included ~6 million data (observed at ~2300 stations) in the relocation procedure, including ~146,000 CC differential times and ~348,000 depth phase observations.

[11] To properly account for the varying data quantities, types, and qualities, we applied a hierarchical dynamic

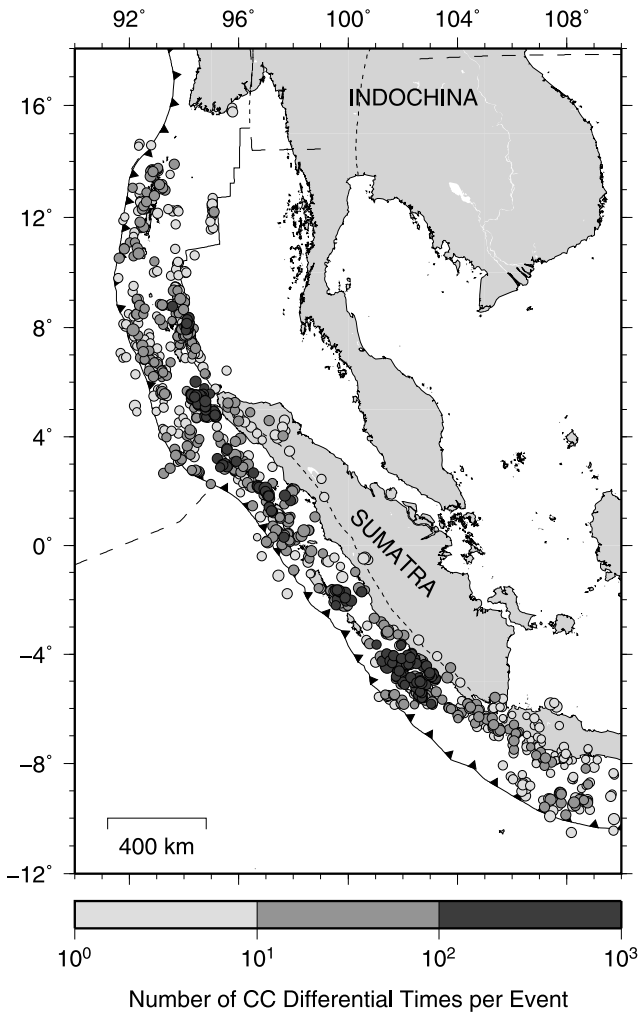

Figure 2. Distribution of ~1200 events from which cross-correlation (CC) data were included in the relocation procedure.

weighting scheme to the data [e.g., *Waldhauser and Ellsworth*, 2000; *Zhang and Thurber*, 2003; *Waldhauser and Schaff*, 2007]. We initially gave the absolute data high weighting, because they control the absolute locations, and then progressively lowered their weighting during subsequent iterations. Conversely, we progressively increased the weighting of the differential times during iterations. The final iterations were performed with the CC differential times weighted the highest to allow these more precise data to control the final locations. This type of weighting scheme allows for initial improvements to the absolute locations using the 3-D velocity model and determination of more precise relative locations due to the use of differential times.

3. Assessment of Relocation Quality

[12] We have successfully relocated ~8000 earthquakes along the Sumatra, Andaman, and Burma subduction zones. However, for assessment of location quality, we focus mainly on the ~1200 events (Figure 2) for which CC data are available (section 3.1), due to the fact that these events are likely to show the most improvement, and on the nine events for which local data are available for inclusion and comparison (section 3.2). We conducted a jackknife uncertainty analysis of these event locations. To compute the uncertainties, we re-computed their locations using 10 different subsets of recording stations, each with 10% of the stations omitted. We then used the relocations from these data subsamples to estimate a covariance matrix and compute 95% confidence intervals [*Aster et al.*, 2005]. The results of these tests provide an estimate of the absolute location uncertainties, which are ~10, 11, and 7 km in longitude, latitude, and depth, respectively (Figure 3). Thus, the absolute location uncertainties are reduced compared to the EHB epicentral (~15 km) and focal depth (~10 km) uncertainly estimates [*Engdahl et al.*, 2007]. The modest reduction in absolute location uncertainly for these events is not unexpected due to the limited resolution of the 3D velocity model, and due to the fact that most of the improvement in location quality due to the use of differential data occurs in relative location precision (discussed in section 3.2) [e.g., *Shearer*, 1997].

3.1. Grid Search Relocation and Validation

[13] For the events for which CC data are available (Figure 2), we have obtained >95% data variance reduction compared to the initial EHB locations and significant improvements to the relative locations. However, other than the reprocessed EHB results of *Engdahl et al.* [2007], there

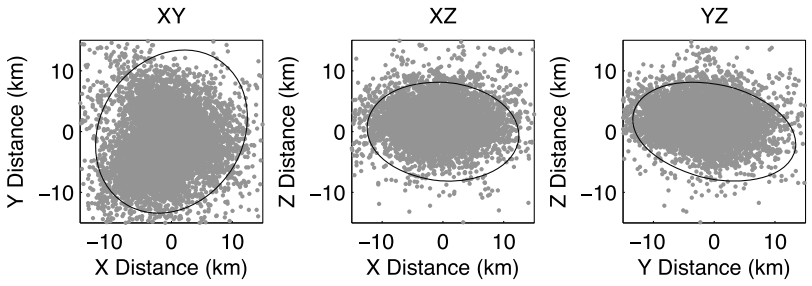

Figure 3. Jackknife uncertainty analysis for events shown in Figure 2. Ten subsamples of recording stations were used, each with 10% of the stations removed, to recompute the locations. The distances shown are deviations from the preferred location (using all stations) for each event. Error ellipses contain 95% of the data points (not all shown). Mean deviations in longitude, latitude, and depth are 10, 11, and 7 km, respectively, and represent estimates of the absolute location uncertainties.

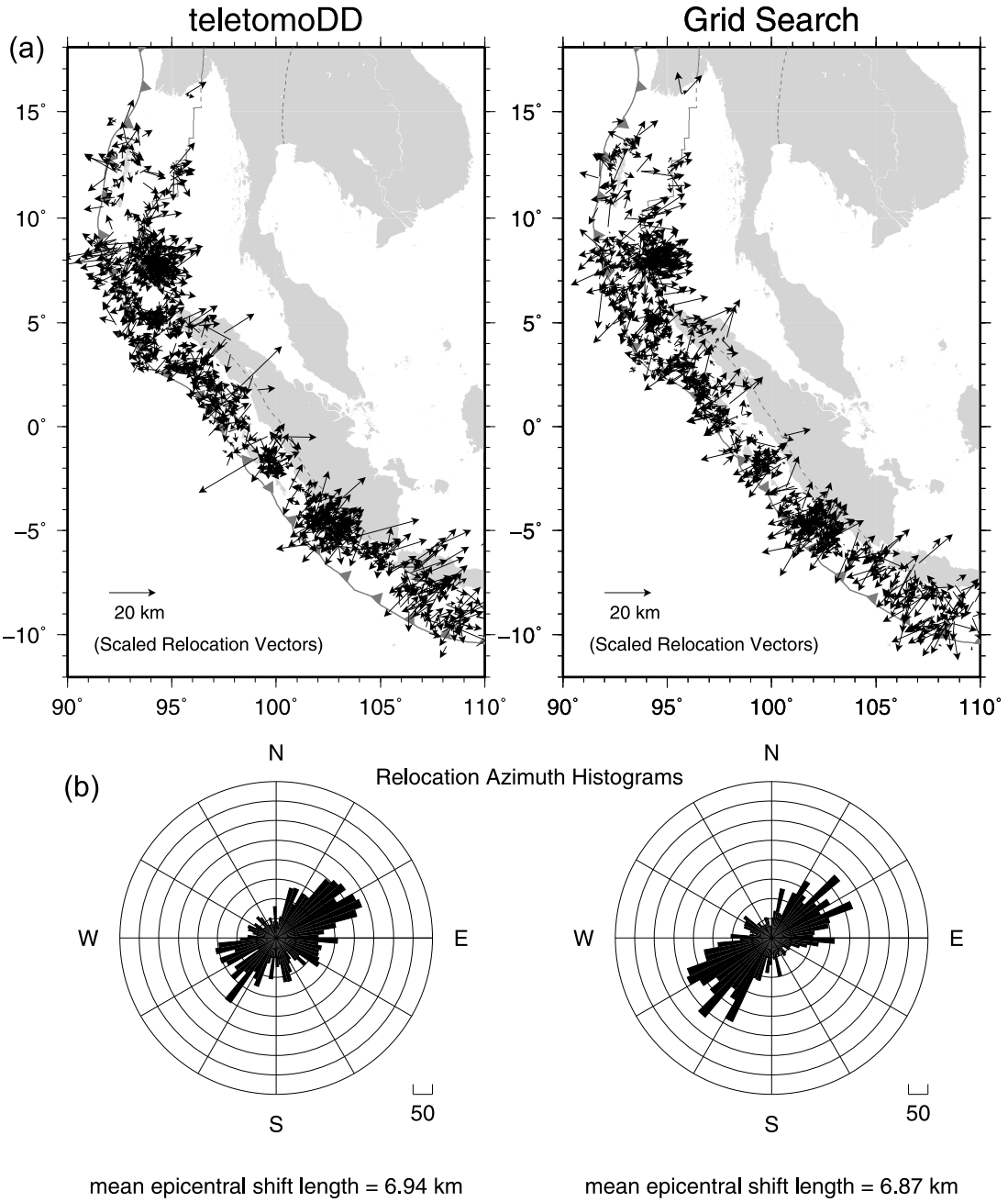

Figure 4. (a) Epicenter shifts relative to EHB locations for the ~1000 events from Figure 2 that have acceptable grid search relocations. Relocations determined by (left) our DD method and (right) our grid search relocation (GS) method. Only grid search vector changes <20 km were accepted (see discussion in text). Note the exaggerated scaling of the relocation vectors. (b) Rose diagrams showing number of relocations for 5° azimuth bins. (c) Depth shifts relative to EHB locations for the same events, plotted as the difference between the EHB depth and the relocated depth versus EHB depth, and (d) histograms showing the number of events per depth shift and the mean shift for the DD and GS relocations. Both methods show a similar trend of migration of epicenters perpendicular to the trench, and consistently shallower depths relative to the EHB depths (at all depths), which can be attributed mostly to the influence of the 3-D velocity model used.

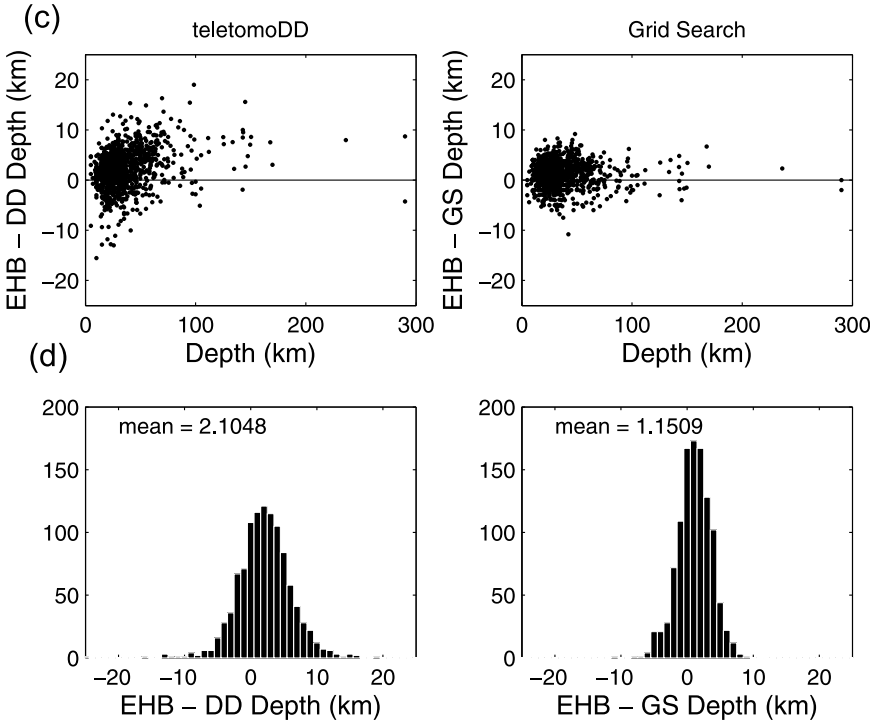

Figure 4. (continued)

are no other comprehensive catalogs available for comparison. Thus, in order to assess the quality and accuracy of the teleseismic DD relocations and to help validate the new *teletomoDD* algorithm, we have developed a grid search relocation technique to verify our results. Using the same ray tracer, phase data, and 3-D velocity model as used in the DD relocation, we calculated travel times for each phase to each point in a grid area around the EHB location and computed an L1 weighted misfit at each grid point. We defined the origin time correction as the weighted average residual of all phases at each point and subtracted it from individual phase residuals prior to calculation of the misfit. The search for the minimum misfit computed in this way was carried out at 0.1° intervals within an initial 1° grid around the EHB hypocenter. The grid was then redefined around the coarse-grid minimum and refined to 0.1° and searched at 0.01° intervals. If the minimum-misfit point was located on a grid edge, the grid was moved and recentered around that minimum and the search was repeated.

[14] Although this grid search scheme will always find a minimum misfit, determination of the global minimum is not guaranteed. Our investigation of the largest relocation changes, those >20 km in length, has shown that the new locations represent local minima and that the global minima were missed due to the discrete sampling of misfit space. However, DD relocations were often found outside the EHB uncertainty (10–15 km). To allow for moderate location changes while minimizing determination of local minima, we chose to accept grid search relocations for location vector changes <20 km.

[15] Using this grid search relocation method, we have accepted relocations for ~1000 (~83%) of the earthquakes in Figure 2 that have refined picks and CC data available. Figure 4 shows a comparison of relocations for these same events obtained with the grid search versus *teletomoDD*. In general, there is good agreement in the pattern of shifts obtained using the two techniques. The mean shifts in epicenter (6.9 km) and depth (2.1 km) are thus significant. Although the shifts are within the original EHB uncertainties, they are systematic. Epicenter shifts trend perpendicular to the trench (Figure 4a), and depths are systematically shallower relative to the EHB locations (Figure 4b). Both sets of relocations show the general migration of epicenters perpendicular to the trench, and the shallowing of depths relative to the initial EHB locations. Overall, hypocenter shifts from the grid search method are comparable to shifts obtained by the DD method, with consistent mean epicenter (Figure 4a) and focal depth shifts (Figure 4b). Differences between these large-scale patterns between the two methods are likely due to the limitations of the grid search scheme, subtle differences in the realization of the velocity models, and the effects of the relative differential data in the DD method. Despite these differences, the general agreement between the results gives us confidence that the systematic relocation shifts we have obtained using *teletomoDD* are valid and significant and are due in large part to the use of a realistic 3-D velocity model. In particular, we have determined that the use of a crustal model [CRUST 2.0; *Bassin et al.*, 2000] that includes faster crustal velocities for the oceanic areas relative to *ak135* mostly accounts for the reduced average depth relative to the EHB depths. These results are consistent with depths determined by waveform modeling [*Tilmann et al.*, 2010] and with biases in the EHB locations determined by com-

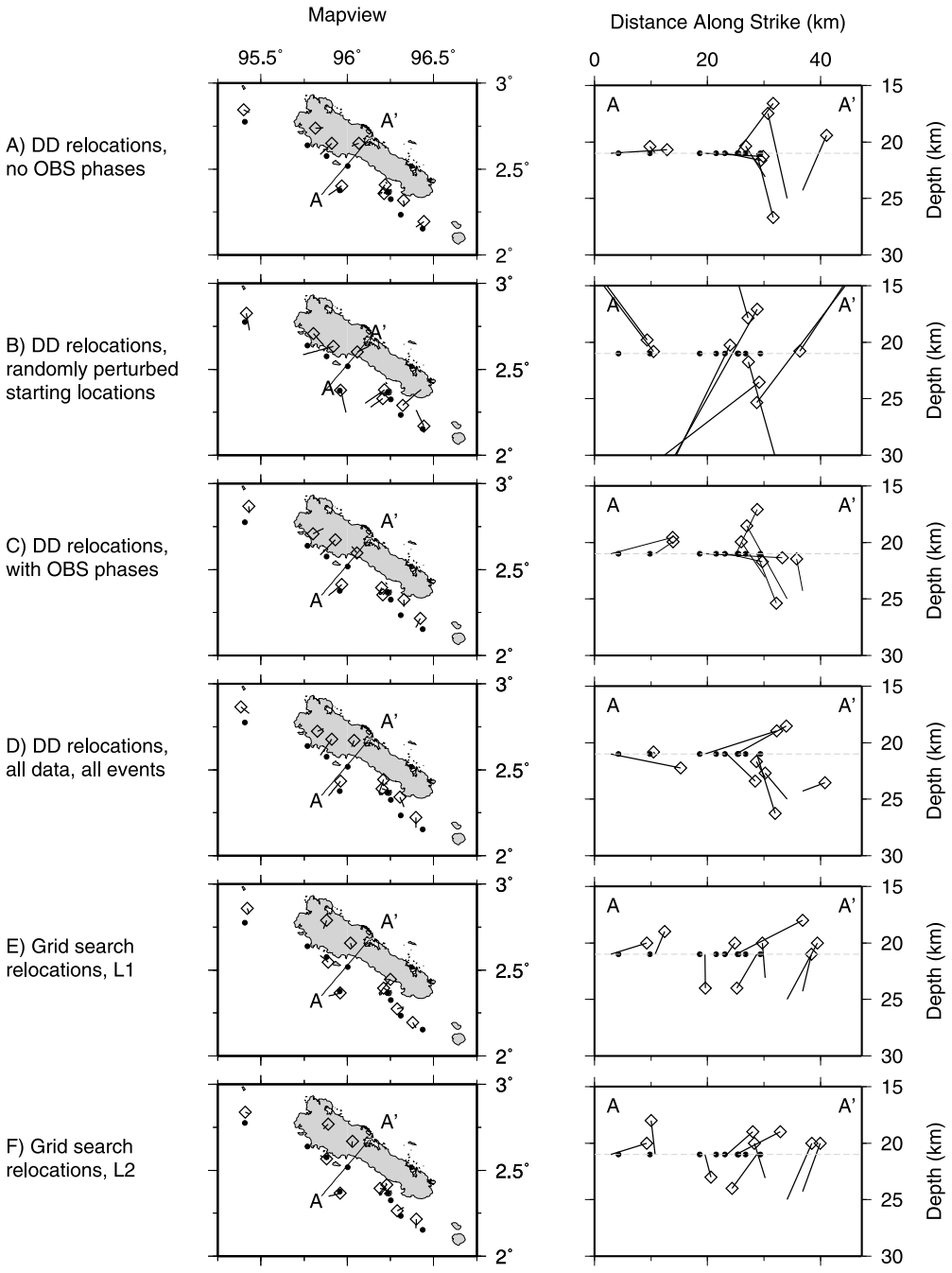

Figure 5. Comparison of locations for nine events near Simeulue Island that were both locally and teleseismically recorded. The locations determined using local data (circles) serve as "ground truth" and help us assess our relocation abilities for the larger catalog of teleseismic events. Lines are shown from the EHB locations (which included the OBS phases) to the new relocations (diamonds), which were determined without the OBS phases. Results are shown for various methods and inclusion or exclusion of various data types. (a) DD relocations (without OBS phases) and (b) randomly perturbed starting locations. (c) DD relocations with OBS phases and (d) DD relocations extracted from the complete relocation catalog where differential times formed between other events are also used in the relocation. (e) Grid search relocations where the L1 norm was minimized and (f) where the L2 norm was minimized. (g) DD relocations when the crustal layer (CRUST 2.0) [*Bassin et al.*, 2000] was excluded from the 3-D model used for ray tracing, (h) when all depth phases are excluded, (i) when all differential times are excluded, and (j) when all absolute data are excluded. Figures 5a–5f illustrate the stability of the relocations and the ability of *teletomoDD* to properly constrain focal depth in the absence of local data. Figures 5g–5j illustrate the importance and influence of each of the data types and an accurate near surface velocity model (see also discussion in text).

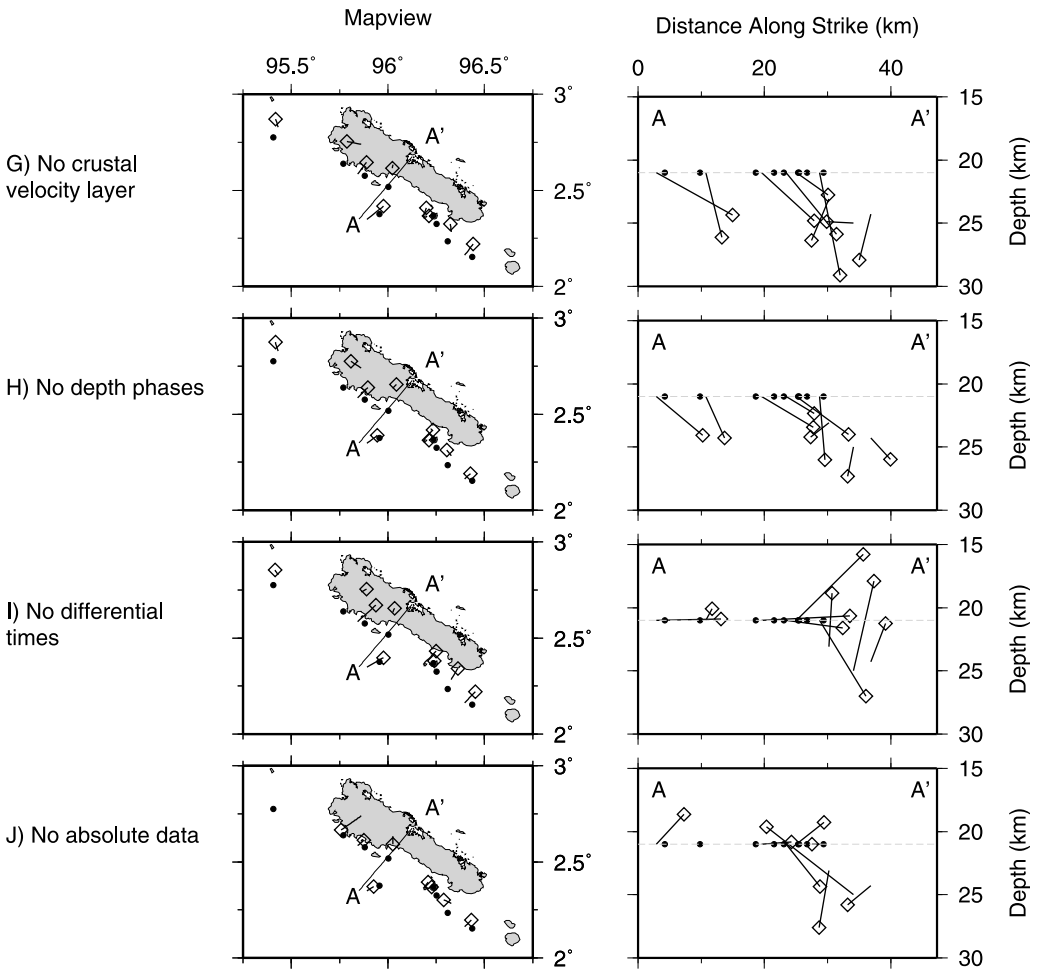

Figure 5. (continued)

parison to local OBS locations for common events [*Tilmann et al.*, 2010; *Araki et al.*, 2006].

3.2. Comparison to OBS Determined Locations: "Ground Truth"

[16] Although local data are absent for much of the region surrounding the rupture areas of the 2004 and 2005 great earthquakes, data from several temporary OBS deployments are or will become available for comparison with our teleseismic relocations. A set of nine teleseismically recorded events that occurred near Simeulue Island was also recorded using OBS stations in the vicinity of the epicenters [*Tilmann et al.*, 2010]. Phase data from the OBS stations were used to relocate the nine events using a multiple event location method and a local 3-D velocity model [*Tilmann et al.*, 2010]. The depths of these nine events were determined to lie on a fault at 21 km depth. We consider these locations, derived from local data, as the most accurate locations available. They are the closest we can get to actual "ground truth" known locations. Thus, they can be used to calibrate and assess our teleseismic relocation procedure, in particular, the ability of *teletomoDD* to determine focal depth.

[17] In Figure 5, we show 10 sets of relocation results for these nine events performed in various ways. For eight of the sets of relocations Figures 5a–5d and 5g–5j, we have altered some part of the DD relocation procedure to examine its effect on the results. For comparison, we also show two sets of relocations for the nine earthquakes using our grid search method Figures 5e–5f. The results show that epicentral changes to the EHB locations are relatively small and stable despite exclusion of the OBS phases. In addition, the results are significant because they illustrate the importance of the various aspects of the relocation procedure for constraining focal depth. Assuming that the locally determined depth of 21 km is correct, it is clear from the results that the inclusion of the depth phases, differential times, and a reasonably accurate crustal velocity structure are each necessary to properly constrain the depths of these events using only teleseismic data. Removing the crustal layer or the depth phases (Figures 5g–5h) causes the events to locate consistently deeper than 21 km. Relocation of these events using all available data and an appropriate 3-D velocity model recovers the depths better (Figure 5d), even when the starting locations are significantly perturbed (Figure 5b). In addition, the relocations are well constrained despite the absence of

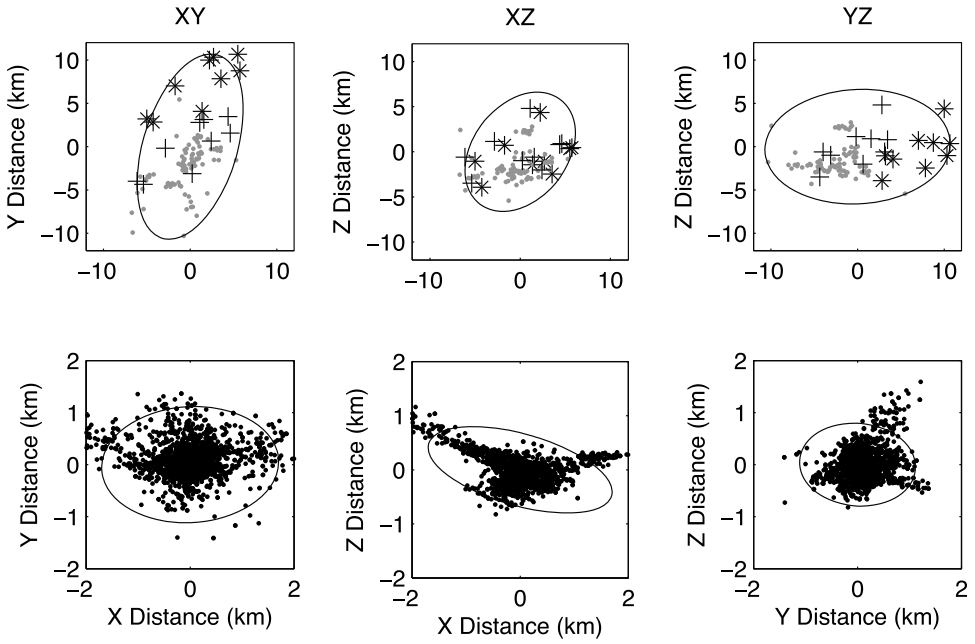

Figure 6. (top) Jackknife uncertainty analysis (see also Figure 3) for the nine ground truth (GT) events discussed in text (see also Figure 5). Gray circles are the 10 (90 total) station subsample deviations from the preferred location, asterisks are the deviations from the GT locations, and crosses are the deviations from the GT locations with the average GT location bias removed. Mean deviations in longitude, latitude, and depth are 4.9, 8.6, and 5.3 km, respectively, and represent estimates of the absolute location uncertainties for these nine events. (bottom) Bootstrap uncertainty analysis for the nine GT events. Random Gaussian noise with a standard deviation of 0.5 s was added to the travel times and the locations were recomputed 200 times (1800 data points). Mean deviations in longitude, latitude, and depth are 1.4, 0.9, and 0.6 km, respectively, and represent estimates of the relative location uncertainties for these nine events.

CC data (only two CC differential times exist for the nine events). Thus, when applied to the larger catalog of events, we can infer that our process will improve the accuracy of the locations. Other local data sets can be used to further assess our results when they become available [e.g., *Lin et al.*, 2009].

[18] The jackknife uncertainty estimates obtained for these events are 5, 9, and 5 km for longitude, latitude, and depth, respectively (Figure 6, top). From Figures 5 and 6, there appears to be a bias in the DD epicenters with respect to the locally determined epicenters. However, the bias is mostly contained within the 95% absolute uncertainty ellipses. Removing the average bias (~7 km) produces the expected typical location scatter about the DD locations (Figure 6, top). In addition to the jackknife analysis, we have also performed a bootstrap uncertainty analysis to estimate relative location uncertainties [e.g., *Shearer*, 1997; *Waldhauser and Ellsworth*, 2000] (Figure 6, bottom). We added random Gaussian noise with a standard deviation of 0.5 s to the travel times and recomputed each of the nine locations 200 times. Estimates of the relative location uncertainties for longitude, latitude, and depth due to random pick errors are 1.4, 0.9, and 0.6 km, respectively. The bootstrap results illustrate the ability of DD methods to minimize the influence of pick errors and produce precise relative earthquake locations.

4. Discussion

[19] Our results illustrate the advantages of teleseismic relocation using *teletomoDD*, which combines advantages of absolute relocation using a realistic 3-D velocity model with the advantages of relative relocation using differential

Figure 7. (a) Map view of DD relocations for the entire EHB catalog of ~8000 events. Cross-section locations for Figures 7b and 7c are also shown. Volcanoes are shown as triangles. (b) Example cross sections showing significant differences in the DD locations versus EHB locations. Although improvements to the locations are subtle at this scale, these cross sections show marked improvement to slab definition. Seismicity in the Burma region (sections 1 and 2) was not reanalyzed by *Engdahl et al.* [2007]. Thus, the DD relocations here show greater improvements than elsewhere in the study region. In the region of the epicenters of the 2004 and 2005 great earthquakes (sections 11 and 12), significant improvements to slab definition are also achieved. Volcano locations are shown as triangles above sections where present. (c) DD relocations for all sections shown in Figure 7a overlain on the Vp model of *Pesicek et al.* [2010], shown as velocity perturbation relative to the reference model.

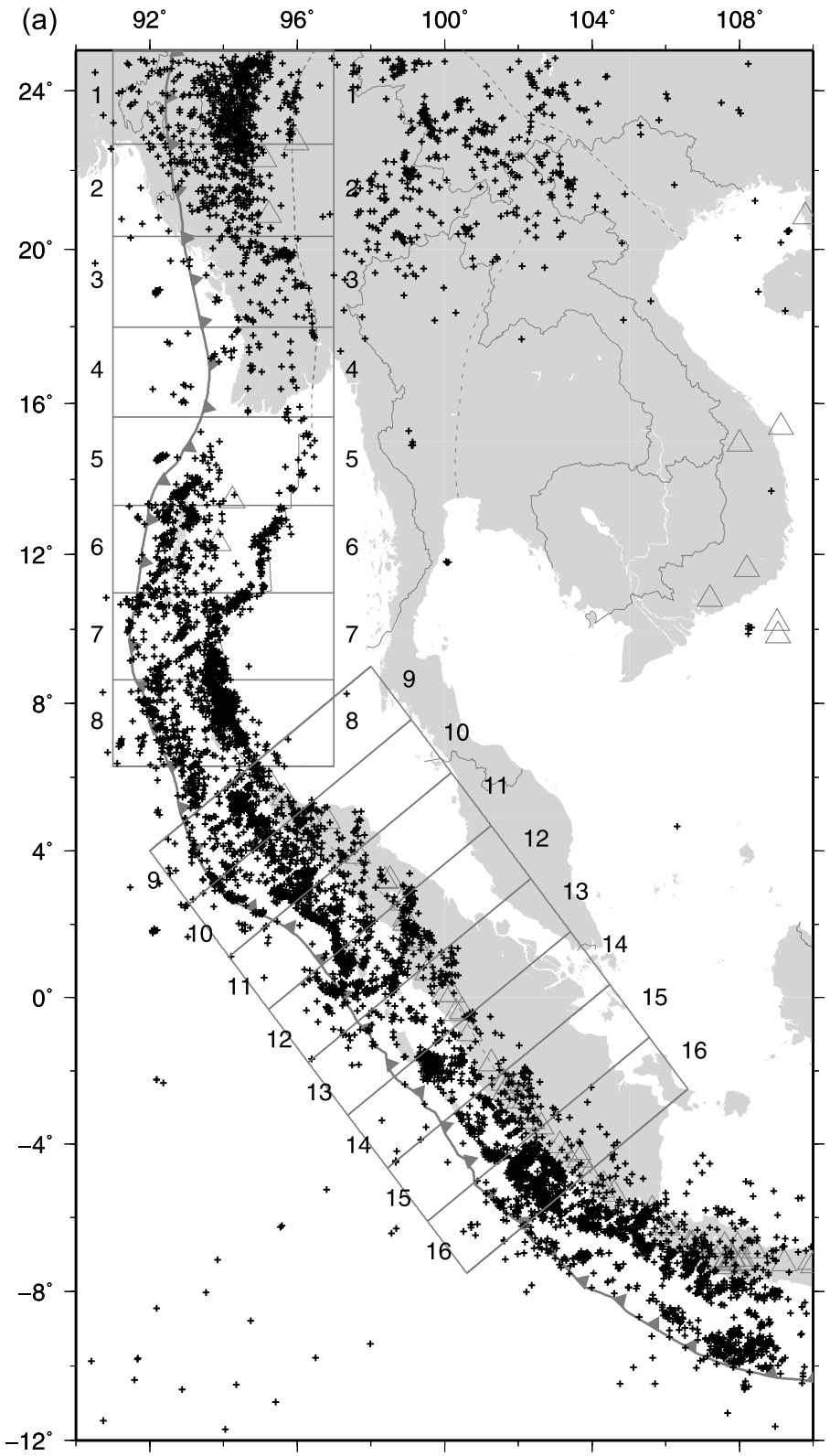
(a)
92°
96°
100°
104°
108°
24°
20°
16°
12°
8°
4°
0°
−4°
−8°
−12°
1
2
3
4
5
6
7
8
9
10
11
12
13
14
15
16

Figure 7

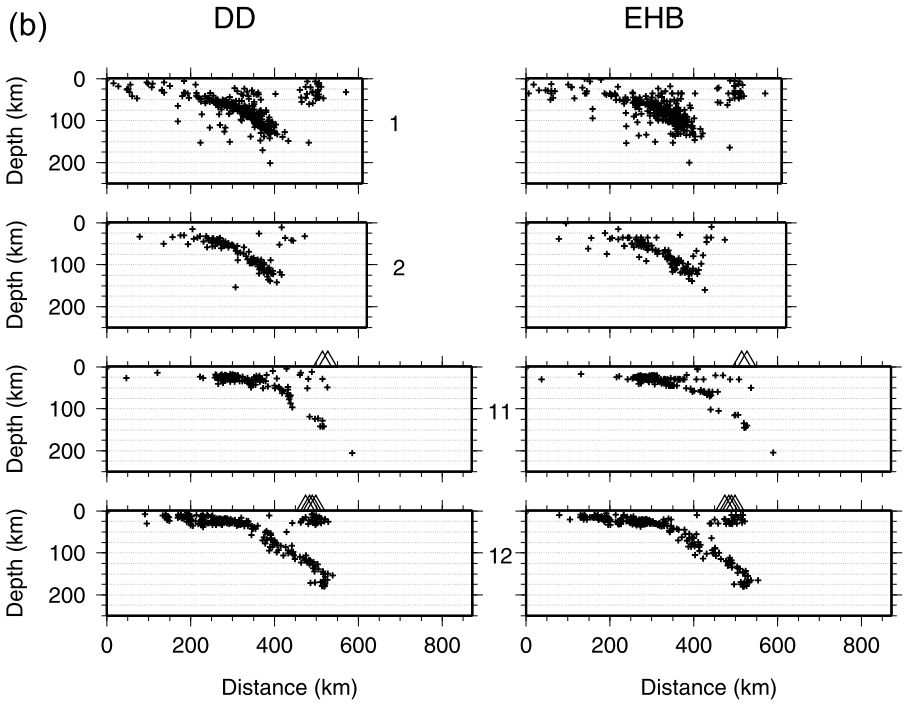

Figure 7. (continued)

times. Not only have we obtained more accurate absolute locations where systematic shifts have presumably reduced regional biases, but we have also obtained improvements to the relative locations of the events, visible in the decreased scatter in the new locations, which better define slab geometry (Figure 7). In addition, events whose depths were previously poorly constrained by the EHB method and were thus assigned fixed depths, now have free depth solutions constrained by the differential times, eliminating the horizontal linear artifacts apparent in some cross sections of EHB seismicity (Figure 7b). In Figure 7c, we have overlain the relocations on the 3-D velocity model used for relocation [*Pesicek et al.*, 2010]. The parameterization and resolution of the tomography model (~50 km) cause the images to have a rather blocky depiction at this scale that results in a mismatch between seismicity on the megathrust and the position of the top of the slab in some cross sections. However, the new locations and velocity model, both derived from teleseismic data, together provide the most comprehensive view of the large-scale structure of this subduction zone yet available [cf. *Widiyantoro and van der Hilst*, 1996; *Shapiro et al.*, 2008] (Figure 7c), with a resolution approaching that which can be obtained using regional/local data.

[20] At a smaller scale, our refined locations in the region of the bend in the trench and the area surrounding the rupture zones of the 2004 and 2005 great earthquakes (Figure 8) provide better constraints on the aftershock distribution and its relation to prior seismicity and coseismic slip. Events prior to the 2004 earthquake mostly locate downdip of slip from the 2004 event and away from the trench (Figure 9) [see also *Engdahl et al.*, 2007]. In contrast, aftershocks mostly occur surrounding the areas of high coseismic slip [*Ishii et al.*, 2005], including many events at or near the trench. In addition, the relocations show that several segments of the Sumatra strike-slip and Andaman backarc faults were inactive following the 2004 event, but one segment in particular, centered at ~94°E and ~8°N, became very active [e.g., *Dewey et al.*, 2007; *Engdahl et al*, 2007].

[21] In the region surrounding the rupture of the 2005 event, seismicity is again lacking in the rupture zone prior to the event and is concentrated along its boundaries after the event (Figure 10). Aftershocks located at the updip limit of coseismic slip define a narrow zone of seismicity, at depths of ~15–30 km, across the entire rupture area. We assume that the majority of these aftershocks occur on the megathrust and that their curvilinear trend in mapview reflects the shape of the megathrust in this region. Their trend is also consistent with that of the trench, volcanic arc, and the subducting slab (Figure 11). The fold in the slab inferred from local [*Fauzi et al.*, 1996] and teleseismic earthquake locations to exist at depths as shallow as 75 km and extend through the upper mantle and into the transition zone from tomography results [*Pesicek et al.*, 2008, 2010] is also expressed in the shape of the megathrust (Figure 11) and is thus a primary feature of the downgoing plate.

[22] The tight clustering of these events at the updip limit of coseismic slip may be revealing a mechanical barrier to rupture on the megathrust. Alternatively, it may be a frictional transition. If such a barrier exists here, slip from the 2005 event would have concentrated stress along it. This stress was subsequently relaxed by the aftershocks (Figure 10), which may have been driven by aseismic afterslip that was observed updip of the rupture zone all the way to the trench [*Hsu et al.*, 2006]. This barrier may also have

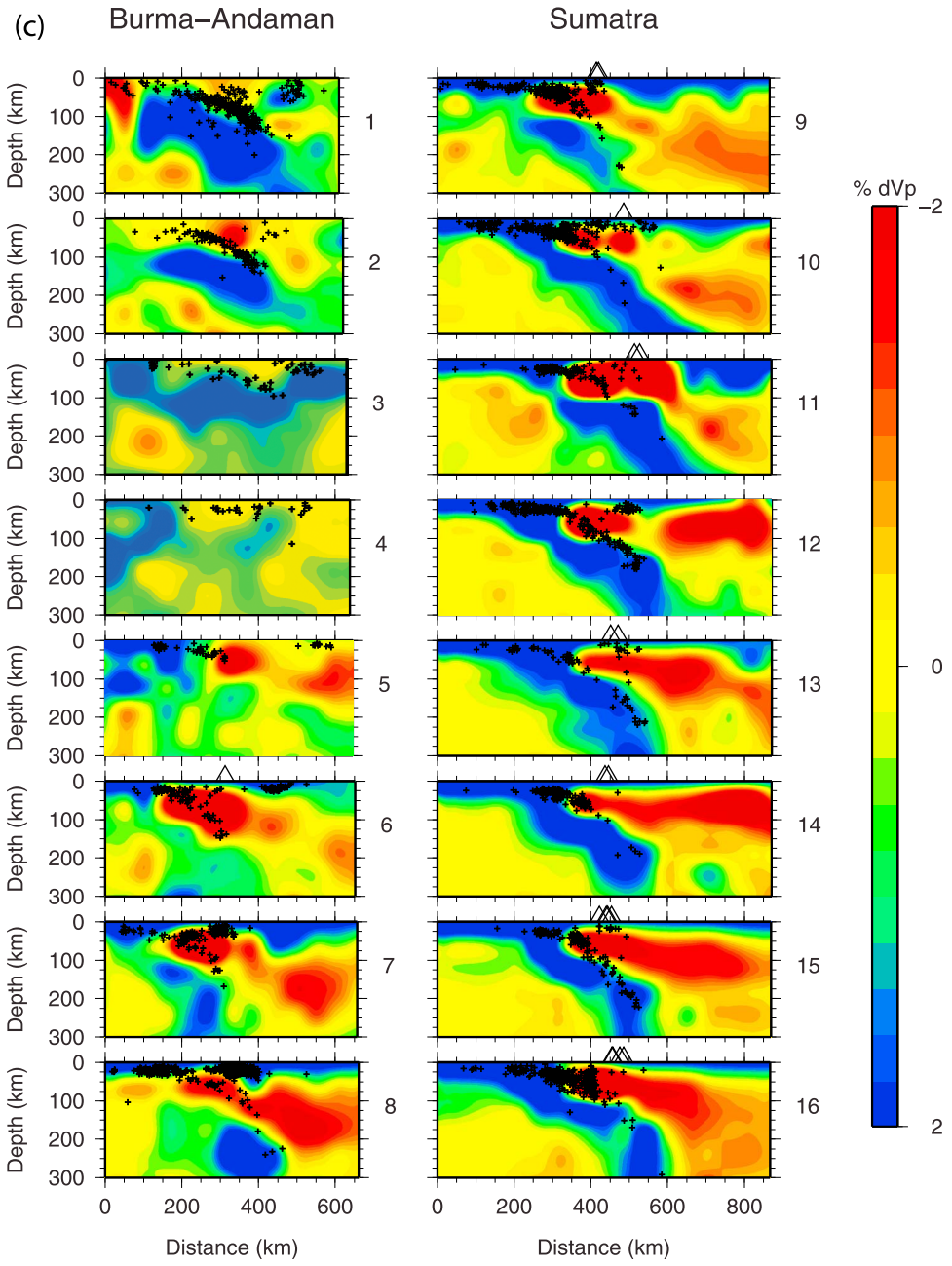

Figure 7. (continued)

contributed to the lack of a significant tsunami caused by the 2005 event. Unfortunately, published local bathymetric and reflection data in the region [*Henstock et al.*, 2006; *Sibuet et al.*, 2007; *Singh et al.*, 2008; *Franke et al.*, 2008] do not extend far enough south to cover the area where these events occurred, so the nature of this feature remains uncertain.

[23] North of this arcuate seismic feature and directly north of Simuelue Island, good local seismic and bathymetric coverage does exist. The epicenter of the 2004 event and the southern boundary of the Andaman microplate are in this region. Reflection and bathymetric studies of this area have revealed the locations of many splay and backthrust faults [*Henstock et al.*, 2006; *Sibuet et al.*, 2007; *Singh et al.*, 2008]. Relocations of a group of aftershocks following the 1976 M7 event, thought to have ruptured a small forearc fault [*DeShon et al.*, 2005], now show a geometry indicative of a backthrust (Figure 12), which may be the deeper extension of a backthrust imaged landward of the West Andaman Fault in the same region by *Singh et al.* [2008].

[24] Patterns of seismicity in this area may be reflecting plate structures that influence rupture segmentation on the megathrust. There is good spatial correspondence between a gap in seismicity below the center of Simuelue Island (Figure 12) and the saddle-shaped region of minimal uplift between the 2004 and 2005 ruptures discussed by *Briggs et al.* [2006]. This gap is also prominent in local OBS after-

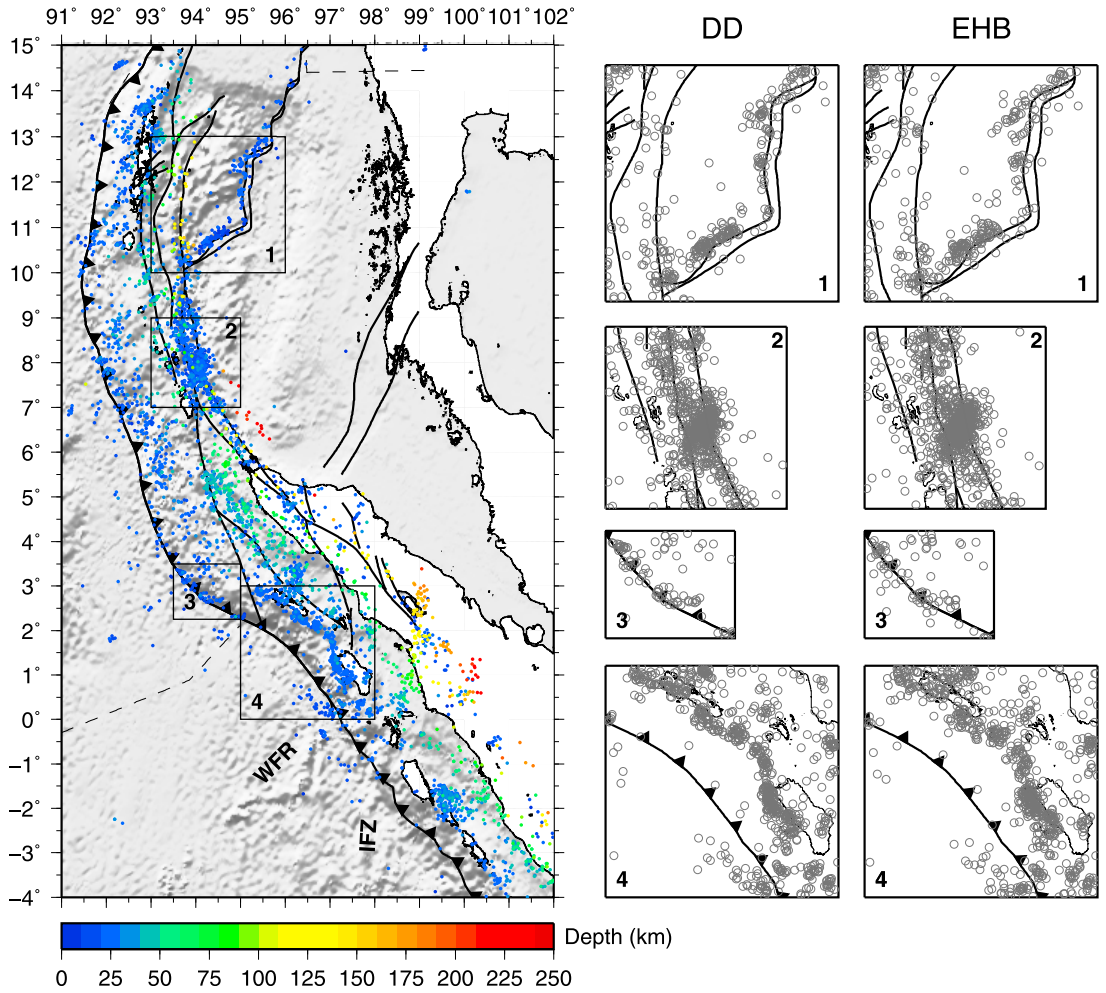

Figure 8. DD relocations for the region surrounding the bend in the trench and the rupture areas of the 2004 and 2005 great earthquakes. Fault locations (black) are from *Curray* [2005]. Spatial refinement of locations is visible along the Andaman Sea backarc spreading-related faults (1 and 2), at the trench offshore north, Sumatra (3) and landward of the bend in the trench near Simeulue and Nias Islands (4) (see also Figures 10 and 11).

shock locations [*Tilmann et al.*, 2010]. On the basis of seismic refraction studies, *Franke et al.* [2008] propose a buried fracture zone below Simuelue as a cause for rupture segmentation between the 2004 and 2005 events. They cite EHB locations directly north of Simuelue as possibly supporting the presence of such a feature. Our relocations of these events show the same rough NNE trend but neither bolster nor refute their claim. If there is fracture zone subducting here, it seems to be aseismic beneath Simuelue but active directly north of it.

[25] A fracture zone that is apparent in our relocations is the Investigator Fracture Zone (IFZ). The IFZ subducts outboard of Siberut Island (Figure 11). This highly seismic feature may be the source of a small tear in the slab below Toba Caldera [*Page et al.*, 1979; *Fauzi et al.*, 1996]. The DD relocations image this feature quite well (Figures 8 and 11) and are in good agreement with the local earthquake locations of *Fauzi et al.* [1996]. In addition, the location of the seismicity on the IFZ correlates with a change in the geometry of the slab visible in tomography results. Figure 13 shows an apparent discontinuity, possibly vertical offset, in the fast slab that correlates with the seismicity of the IFZ. Although the parameterization of the tomography model (~50 km) is rather coarse relative to this feature, resolution in this region at these depths is good [*Pesicek et al.*, 2010], and is aided by local data from a temporary seismic network deployed around Toba Caldera [*Fauzi et al.*, 1996]. The offset of slab anomalies suggests an east-side up sense of motion, as would be expected if the IFZ was accommodating arc parallel shear stress due to oblique convergence. However, available fault plane solutions for these events do not help to clarify what sense of motion might exist along the IFZ (Figure 13; see also *Fauzi et al.* [1996]).

[26] Alternatively, the apparent offset in the slab (Figure 13) could be a result of slab weakening associated with subduction of the Wharton fossil ridge (WFR) and imaged as a region of low velocity. *Eberhart-Phillips et al.* [2006] suggest that a preexisting structural feature subducting beneath

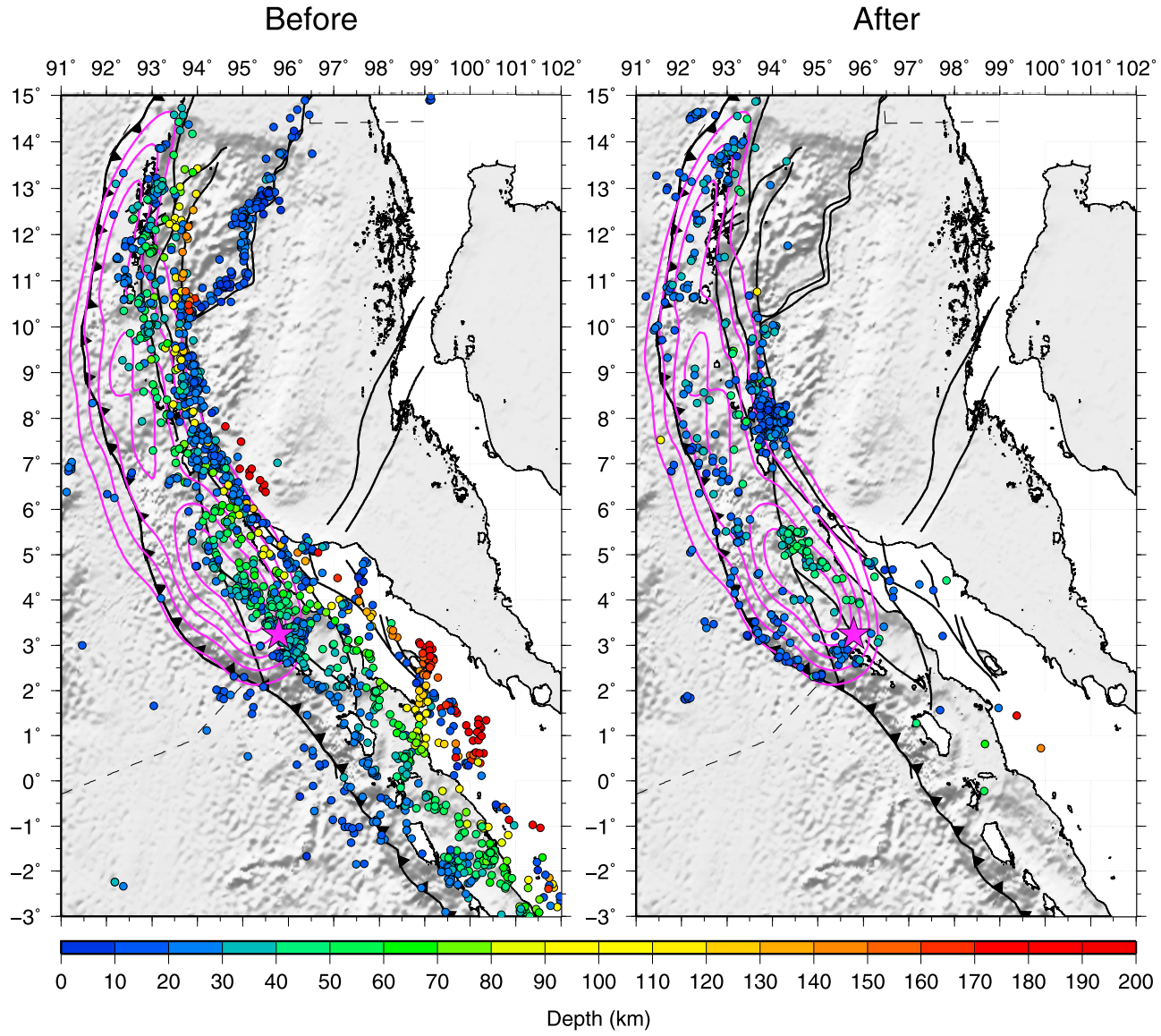

Figure 9. (left) Map of all DD relocations prior to the 2004 M9 event (11 January 1964 through 24 December 2004) and (right) events following the 2004 earthquake but prior to the 2005 earthquake (25 December 2004 through 28 March 2005). Magenta lines represent normalized cumulative radiated energy during the 2004 mainshock displayed from 0.5 to 1.0 at increments of 0.1 [*Ishii et al.*, 2005]. Aftershocks of the 2004 event show good correlation with regions of low coseismic slip, while seismicity prior to the event occurs mostly downdip of the coseismic slip.

central Alaska may be responsible for a similar low-velocity feature imaged there. What, if any, interaction there is between the WFR and the IFZ on the downgoing plate below Sumatra and the broad slow anomalies we have imaged beneath Toba Caldera (also imaged by *Koulakov et al.* [2009]) is unknown. The WFR appears to be relatively aseismic. It is possible that the IFZ and/or WFR, or the interaction of the two, causes a weakness in the slab visible as a low velocity feature in Figure 13, which might also be related to volcanism at Toba Caldera.

[27] The IFZ may also limit rupture propagation in the region, as suggested by *Fauzi et al.* [1996]. Although most coseismic slip from the 2005 event ceased just south of Nias Island [*Briggs et al.*, 2006] (Figure 10), significant afterslip occurred directly south of the coseismic slip [*Hsu et al.*, 2006], filling in the gap between Nias Island and the Batu Islands, which lie directly above the inferred location of the IFZ on the megathrust (Figure 11). Slip in the region of the Batu Islands apparently did occur during a 1935 Mw 7.7 event, but it does not seem to be laterally extensive, and no other historical event can be considered to have ruptured across the IFZ [*Briggs et al.*, 2006; *McCaffrey*, 2009]. In addition, the IFZ and the region near Siberut Island were relatively quiet seismically following the 2004 and 2005

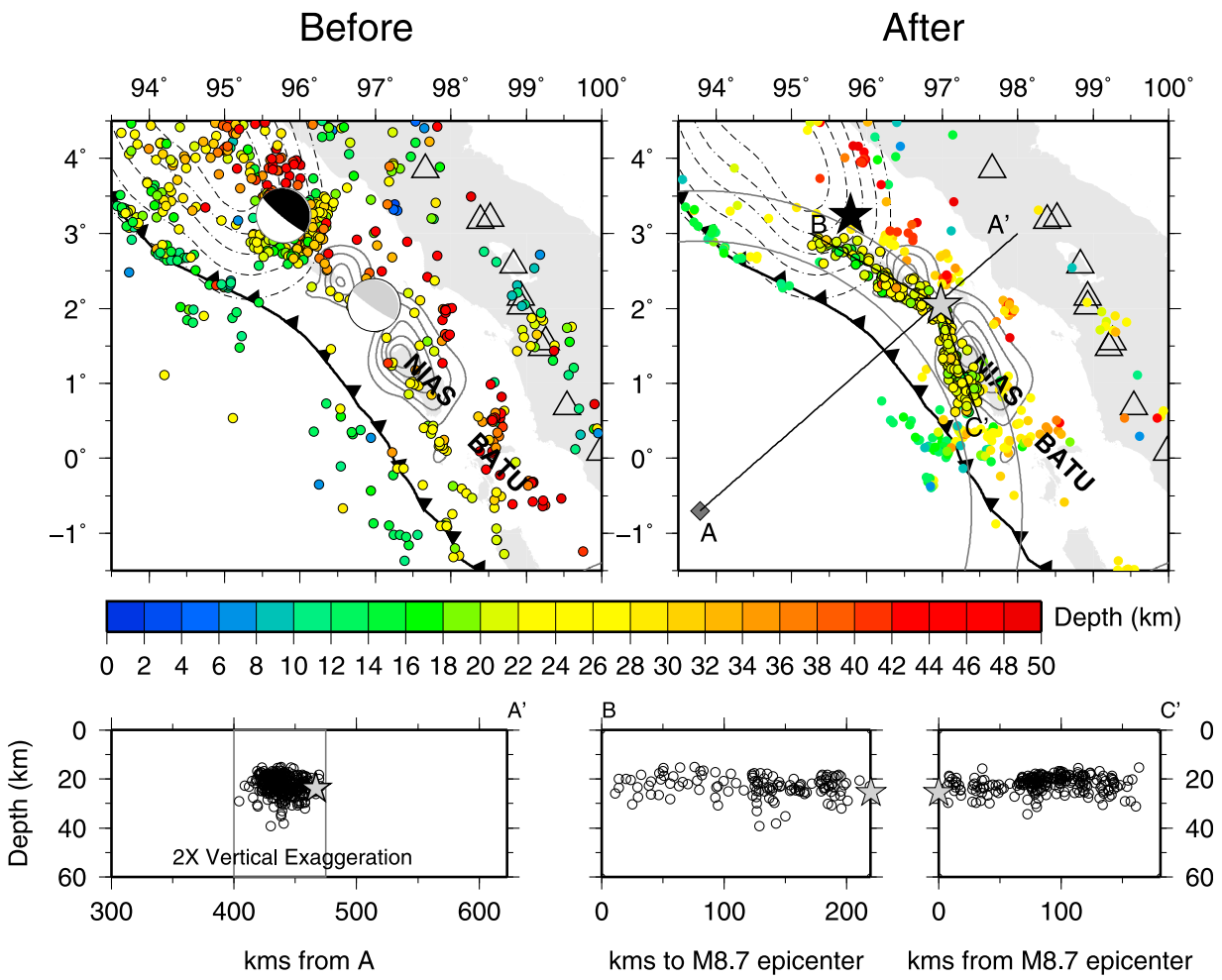

Figure 10. Map of events shallower than 50 km depth occurring (top left) before (11 January 1964 through 28 March 2005) and (top right) after (28 March 2005 through 25 October 2007) the 28 March 2005 M8.7 Nias Island earthquake. The relocations reveal a curvilinear feature on the megathrust that became seismically active after the 2005 event and shows an orientation similar to that of the trench; in addition, it is highly correlated with the boundaries of coseismic slip (contours; 2 m contour interval) of the 2005 event [*Hsu et al.*, 2006]. Dotted contours show slip during the 2004 event (see also Figure 9). Figure 10 (top left) CMTs and Figure 10 (top right) epicenters (stars) for the 2004 (black) and 2005 (gray) events are also shown at their new locations. (bottom) Cross sections of the subset of aftershocks that make up the arcuate feature (shown in top right frame between the two gray concentric arc segments as black outlined circles). (bottom left) Distance from the circle center at A (gray diamond). (bottom middle and bottom right) Along strike views centered on the 2005 epicenter.

events (Figure 11), suggesting that stress release from these two events did not affect the area directly south of the IFZ.

5. Summary

[28] We have successfully relocated ~8000 earthquakes along the Sumatra, Andaman, and Burma subduction zones using a teleseismic DD method with a 3-D velocity model using absolute and differential times for primary and depth phases that improves both absolute locations and relative locations. For our best constrained events, average shifts relative to reprocessed EHB locations [*Engdahl et al.*, 2007] are ~6 km in epicenter and ~2 km in depth and estimated relative location uncertainties are less than 2 km. There are systematic epicenter shifts perpendicular to the trench, while depths are consistently shallower than the EHB locations. In addition to better defining slab and megathrust geometry by decreasing location scatter, several key structural features are well defined by the relocations, including the IFZ, warping of the megathrust, Andaman backarc faults and other faults in the region at shallow depths. These and other features of the relocations may require refinement of previous interpretations in several studies where the conclusions were based in part on EHB locations in the region. Future work will focus on further refining locations and velocity structure jointly and at a finer scale. In the process, we hope to incorporate other new local data sets to increase data coverage and provide further "ground truth" assessment of our results.

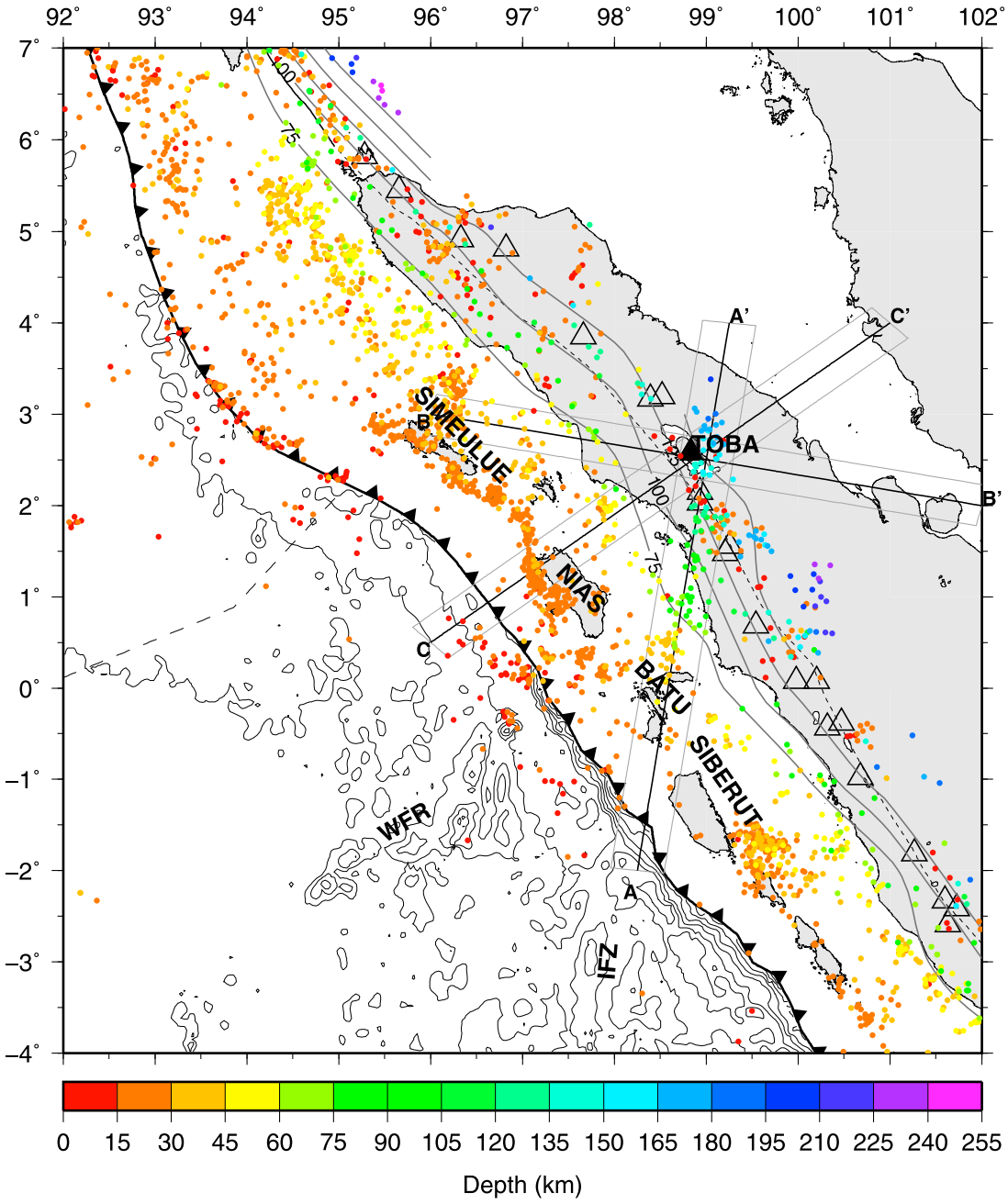

Figure 11. DD relocations (11 January 1964 through 25 October 2007) and slab depth contours constructed for events with depth >50 km. The slab contours (25 km interval) illustrate the broad curvature and the shallower dip of the slab beneath northern Sumatra. Also shown are the locations for cross sections shown in Figure 13 (a) along and (b) perpendicular to the location of the IFZ and (c) perpendicular to the trench. Bathymetry contours (500 m interval) outside of the trench illustrate the location and orientation of the IFZ and WFR. Also shown are volcano locations (triangles) and the Sumatra fault (dashed line).

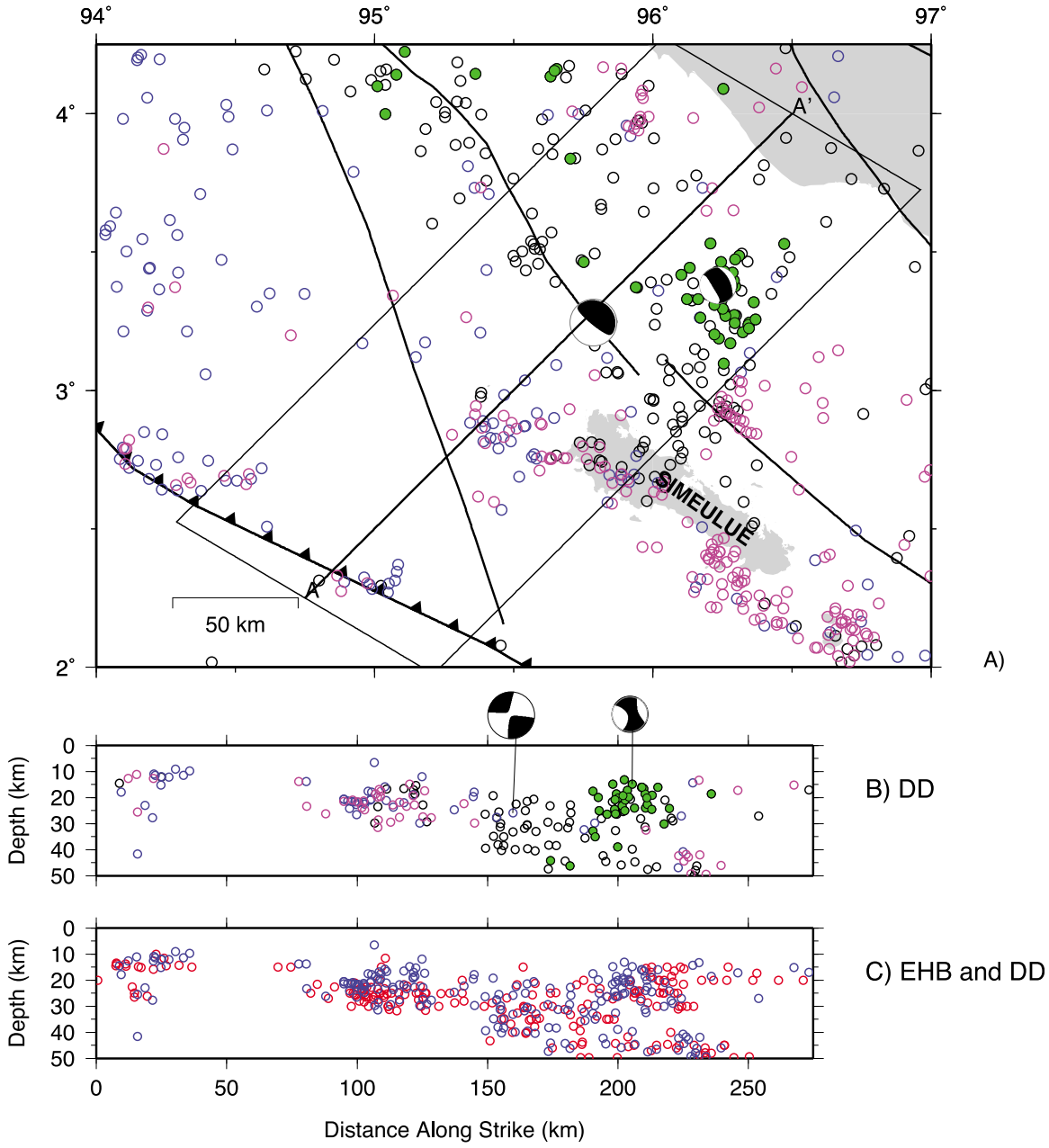

Figure 12. DD relocations of events near Simeulue Island and the 2004 great earthquake. (a) Mapview relocations for events before the 2004 event (black), after the 2004 event but before the 2005 event (blue), and after the 2005 event (blue). CMT solutions for the 2004 M9 and the 1976 M7 events are also shown at their DD locations. Aftershocks of the 1976 event are shown in green. Fault locations (black) are from *Curray* [2005]. Events within the box are projected onto line A-A' and (b) shown and (c) compared to EHB locations. Relocations of the 1976 M7 event and its aftershocks (green) indicate that they likely locate on a backthrust in the region.

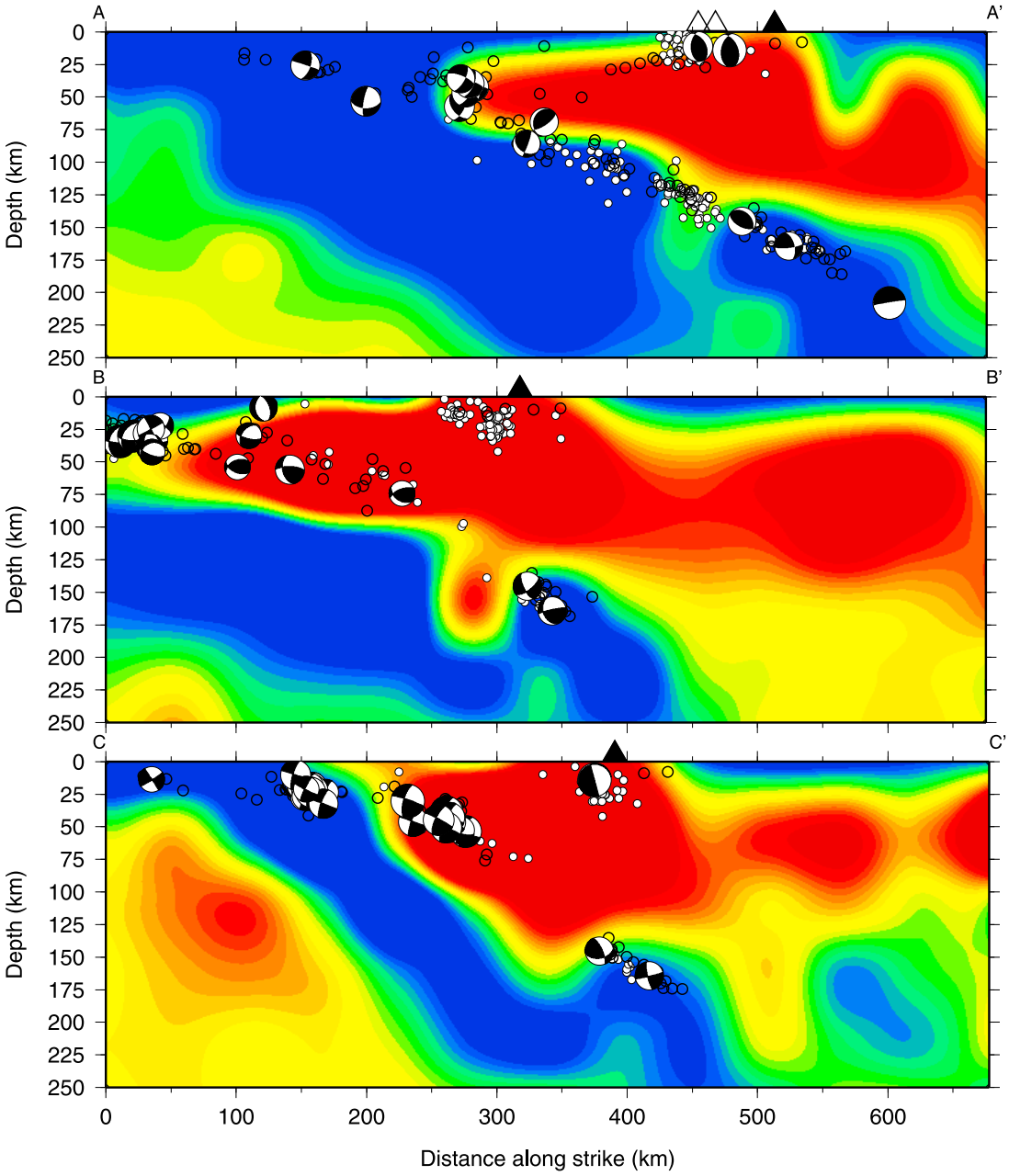

Figure 13. Cross sections (locations shown in Figure 11) (a) parallel and (b) perpendicular to the location of the IFZ and (c) perpendicular to the trench showing teleseismic DD locations (black open circles) and local seismicity recorded by *Fauzi et al.* [1996] (white circles) overlain of the tomography model of *Pesicek et al.* [2010] (velocity scale shown in Figure 7c). The cross sections illustrate a change in the slab velocity anomaly that correlates with seismicity on the IFZ beneath Toba Caldera (black triangle). Other volcanoes (white triangles) and well`constrained global CMTs within each cross section are also shown.

[29] **Acknowledgments.** We thank Frederik Tilmann and an anonymous reviewer for critical reviews. This material is based upon work supported in part by the National Science Foundation under grants EAR-0608988 (H.D. and C.T.) and EAR-0609613 (E.E.) and by NASA, under award NNX06AF10G (C.T.). The data were provided by the ISC and NEIC.

References

Araki, E., M. Shinohara, K. Obana, T. Yamada, Y. Kaneda, T. Kanazawa, and K. Suyehiro (2006), Aftershock distribution of the 26 December 2004 Sumatra-Andaman earthquake from ocean bottom seismographic observation; The 2004 Great Sumatra earthquake and tsunami, *Earth, Planets, Space*, *58*, 113–119.

Aster, R. C., B. Borchers, and C. H. Thurber (2005), *Parameter Estimation and Inverse Problems*, 1st ed., Elsevier, Burlington, Mass.

Bassin, C., G. Laske, and G. Masters (2000), The current limits of resolution for surface wave tomography in North America, *Eos Trans AGU*, *81*, F897.

Briggs, R. W., et al. (2006), Deformation and slip along the Sunda Megathrust in the great 2005 Nias-Simeulue earthquake, *Science*, *311*, 1897–1901.

Curray, J. R. (2005), Tectonics and history of the Andaman Sea region, *J. Asian Earth Sci.*, *25*, 187–232.

DeShon, H. R., E. R. Engdahl, C. H. Thurber, and M. Brudzinski (2005), Constraining the boundary between the Sunda and Andaman subduction systems: Evidence from the 2002 Mw 7.3 Northern Sumatra earthquake and aftershock relocations of the 2004 and 2005 great earthquakes, *Geophys. Res. Lett.*, *32*, L24307, doi:10.1029/2005GL024188.

DeShon, H. R., C. H. Thurber, M. R. Brudzinski, and E. R. Engdahl (2007), A semiautomated technique for waveform cross-correlation of teleseismically recorded depth phases; SSA 2007 meeting announcement; Seismological Society of America, *Seismol. Res. Lett.*, *78*, 242.

Dewey, J. W., G. Choy, B. Presgrave, S. Sipkin, A. C. Tarr, H. Benz, P. Earle, and D. Wald (2007), Seismicity associated with the Sumatra-Andaman Islands earthquake of 26 December 2004, *Bull. Seismol. Soc. Am.*, *97*, 25–42.

Du, W.-X., C. H. Thurber, and D. Eberhart-Phillips (2004). Earthquake relocation using cross-correlation time delay estimates verified with the bispectrum method, *Bull. Seismol. Soc. Am. 94*, 856–866.

Eberhart-Phillips, D., D. H. Christensen, T. M. Brocher, R. Hansen, N. A. Ruppert, P. J. Haeussler, and G. A. Abers (2006), Imaging the transition from Aleutian subduction to Yakutat collision in central Alaska, with local earthquakes and active source data, *J. Geophys. Res.*, *111*, B11303, doi:10.1029/2005JB004240.

Engdahl, E. R., R. D. van der Hilst, and R. Buland (1998), Global teleseismic earthquake relocation with improved travel times and procedures for depth determination, *Bull. Seismol. Soc. Am.*, *88*, 722–743.

Engdahl, E. R., A. Villasenor, H. R. DeShon, and C. H. Thurber (2007), Teleseismic relocation and assessment of seismicity (1918–2005) in the region of the 2004 Mw 9.0 Sumatra-Andaman and 2005 Mw 8.6 Nias Island great earthquakes, *Bull. Seismol. Soc. Am.*, *97*, S43–S61.

Fauzi, R., McCaffrey, D. Wark, Sunaryo, and P. Y. Prih Haryadi (1996), Lateral variation in slab orientation beneath Toba Caldera, northern Sumatra, *Geophys. Res. Lett.*, *23*(5), 443–446, doi:10.1029/96GL00381.

Franke, D., M. Schnabel, S. Ladage, D. R. Tappin, S. Neben, Y. S. Djajadihardja, C. Müller, H. Kopp, and C. Gaedicke (2008), The great Sumatra-Andaman earthquakes—Imaging the boundary between the ruptures of the great 2004 and 2005 earthquakes, *Earth Planet Sci. Lett.*, *269*, 118–130.

Fukuyama, E., W. L. Ellsworth, F. Waldhauser, and A. Kubo (2003), Detailed fault structure of the 2000 Western Tottori, Japan, earthquake sequence, *Bull. Seismol. Soc. Am.*, *93*, 1468–1478.

Henstock, T. J., L. C. McNeill, and D. R. Tappin (2006), Seafloor morphology of the Sumatran subduction zone: Surface rupture during megathrust earthquakes?, *Geology*, *34*, 485–488.

Hsu, Y., M. Simons, J. Avouac, J. Galetzka, K. Sieh, M. Chlieh, D. Natawidjaja, L. Prawirodirdjo, and Y. Bock (2006), Frictional afterslip following the 2005 Nias-Simeulue earthquake, Sumatra, *Science*, *312*, 1921–1926.

Ishii, M., P. M. Shearer, H. Houston, and J. E. Vidale (2005), Extent, duration and speed of the 2004 Sumatra-Andaman earthquake imaged by the Hi-Net array, *Nature*, *435*, 933–936.

Kennett, B. L. N., E. R. Engdahl, and R. Buland (1995), Constraints on seismic velocities in the Earth from traveltimes, *Geophys. J. Int.*, *122*, 108–124.

Koketsu, K., and S. Sekine (1998), Pseudo-bending method for three-dimensional seismic ray tracing in a spherical earth with discontinuities, *Geophys. J. Int.*, *132*, 339–346.

Koulakov, I., T. Yudistira, B. Luehr, and Wandono (2009), *P*, *S* velocity and V_P/V_S ratio beneath the Toba caldera complex (Northern Sumatra) from local earthquake tomography, *Geophys. J. Int.*, *177*, 1121–1139.

Li, C., R. D. van der Hilst, E. R. Engdahl, and S. Burdick (2008), A new global model for *P* wave speed variations in Earth's mantle, *Geochem. Geophys. Geosyst.*, *9*, Q05018, doi:10.1029/2007GC001806.

Lin, J., X. Le Pichon, C. Rangin, J. Sibuet, and T. Maury (2009), Spatial aftershock distribution of the 26 December 2004 great Sumatra-Andaman earthquake in the northern Sumatra area, *Geochem. Geophys. Geosyst.*, *10*, Q05006, doi:10.1029/2009GC002454.

McCaffrey, R. (2009), The Tectonic framework of the Sumatran subduction zone, *Annu. Rev. Earth Planet. Sci.*, *37*, 345–366.

Page, B. G. N., J. D. Bennett, N. R. Cameron, D. M. Bridge, D. H. Jeffery, W. Keats, J. Thaib, J. V. Hepworth, M. G. Audley-Charles, and J. V. Hepworth (1979), A review of the main structural and magmatic features of northern Sumatra; Magmatism and tectonics in SE Asia, *J Geol. Soc. London*, *136*, 569–579.

Pesicek, J. D., C. H. Thurber, S. Widiyantoro, E. R. Engdahl, and H. R. DeShon (2008), Complex slab subduction beneath northern Sumatra, *Geophys. Res. Lett.*, *35*, L20303, doi:10.1029/2008GL035262.

Pesicek, J. D., C. H. Thurber, S. Widiyantoro, H. Zhang, H. R. DeShon, and E. R. Engdahl (2010), Sharpening the tomographic image of the subducting slab below Sumatra, the Andaman Islands, and Burma, *Geophys. J. Int.*, *182*, 433–453.

Prejean, S. G., W. L. Ellsworth, M. D. Zoback, and F. Waldhauser (2002), Fault structure and kinematics of the Long Valley Caldera region, California, revealed by high-accuracy earthquake hypocenters and focal mechanism stress inversions, *J. Geophys. Res.*, *107*(B12), 2355, doi:10.1029/2001JB001168.

Schaff, D. P., G. H. R. Bokelmann, G. C. Beroza, F. Waldhauser, and W. L. Ellsworth (2002), High-resolution image of Calaveras Fault seismicity, *J. Geophys. Res.*, *107*(B9), 2186, doi:10.1029/2001JB000633.

Shapiro, N. M., M. H. Ritzwoller, and E. R. Engdahl (2008), Structural context of the great Sumatra-Andaman Islands earthquake, *Geophys. Res. Lett.*, *35*, L05301, doi:10.1029/2008GL033381.

Shearer, P. M. (1997), Improving local earthquake locations using the L1 norm and waveform cross correlation; application to the Whittier Narrows, California, aftershock sequence, *J. Geophys. Res.*, *102*(B4), 8269–8283, doi:10.1029/96JB03228.

Sibuet, J., et al. (2007), 26th December 2004 great Sumatra-Andaman earthquake: Co-seismic and post-seismic motions in northern Sumatra, *Earth Planet Sci. Lett.*, *263*, 88–103.

Sieh, K., and D. Natawidjaja (2000), Neotectonics of the Sumatran Fault, Indonesia, *J. Geophys. Res.*, *105*(B12), 28,295–28,326, doi:10.1029/2000JB900120.

Sieh, K., D. H. Natawidjaja, A. J. Meltzner, C. Shen, H. Cheng, K. Li, B. W. Suwargadi, J. Galetzka, B. Philibosian, and R. L. Edwards (2008), Earthquake supercycles inferred from sea-level changes recorded in the corals of West Sumatra, *Science*, *322*, 1674–1678.

Singh, S. C., H. Carton, P. Tapponnier, N. D. Hananto, A. P. S. Chauhan, D. Hartoyo, M. Bayly, S. Moeljopranoto, T. Bunting, and P. Christie (2008), Seismic evidence for broken oceanic crust in the 2004 Sumatra earthquake epicentral region, *Nat. Geosci.*, *1*, 777–781.

Tilmann, F. J., T. Craig, I. Grevemeyer, B. Suwargadi, H. Kopp, and E. Flueh (2010), The updip seismic/aseismic transition of the Sumatra megathrust illuminated by aftershocks of the 2004 Aceh-Andaman and 2005 Nias events, *Geophys. J. Int.*, *181*, 1261–1274.

Um, J., and C. H. Thurber (1987), A fast algorithm for two-point seismic ray tracing, *Bull. Seismol. Soc. Am.*, *77*, 972–986.

Waldhauser, F., and W. L. Ellsworth (2000), A double-difference earthquake location algorithm; method and application to the northern Hayward Fault, California, *Bull. Seismol. Soc. Am.*, *90*, 1353–1368.

Waldhauser, F., and W. L. Ellsworth (2002), Fault structure and mechanics of the Hayward Fault, California, from double-difference earthquake locations, *J. Geophys. Res.*, *107*(B3), 2054, doi:10.1029/2000JB000084.

Waldhauser, F., and D. Schaff (2007), Regional and teleseismic double-difference earthquake relocation using waveform cross-correlation and global bulletin data, *J. Geophys. Res.*, *112*, B12301, doi:10.1029/2007JB004938.

Widiyantoro, S., and R. D. van der Hilst (1996), Structure and evolution of lithospheric slab beneath the Sunda Arc, Indonesia, *Science*, *271*, 1566–1570.

Zhang, H., and C. H. Thurber (2003), Double-difference tomography: The method and its application to the Hayward Fault, California, *Bull. Seismol. Soc. Am.*, *93*, 1875–1889.

Zhang, H., and C. H. Thurber (2006), Development and applications of double-difference seismic tomography, *Pure Appl. Geophys.*, *163*, 373–403.

Zhao, D., and J. Lei (2004), Seismic raypath variations in a 3-D global velocity model, *Phys. Earth Planet. Inter.*, *141*, 153–166.

H. R. DeShon, Center for Earthquake Research and Information, University of Memphis, 3890 Central Ave., Memphis, TN 38152, USA.

E. R. Engdahl, Department of Physics, University of Colorado at Boulder, Campus Box 390, Boulder, CO 80309-0390, USA.

J. D. Pesicek and C. H. Thurber, Department of Geoscience, University of Wisconsin-Madison, 1215 W. Dayton St., Madison, WI 53706, USA. (pesicek@geology.wisc.edu)

S. Widiyantoro, Faculty of Mining and Petroleum Engineering, Bandung Institute of Technology, J1. Ganesha, Bandung 40132, Indonesia.

H. Zhang, Department of Earth, Atmospheric and Planetary Sciences, Massachusetts Institute of Technology, 77 Massachusetts Ave., Cambridge, MA 02139, USA.